Research article

Carbon Future

"Redox switches" of Fe species on zeolite catalysts: Modulating the acidity and the para-xylene yield from methanol

Qiongfang Hu[1,#], Hongmei Wang[1,#], Chaojie Cui[1]✉, and Weizhong Qian[1,2]✉

[1] *Department of Chemical Engineering, Tsinghua University, Beijing 100084, China*
[2] *Ordos Laboratory, Inner Mongolia, 017000, China*

Cite This: *Carbon Future*, **2023**, *1*, 9200001

Read Online

ABSTRACT: Molecular switches are widely studied in optical devices, computer science, DNA sensor systems, and chiral synthesis; however, their use in heterogeneous catalytic processes is rarely reported. Herein, we report a Fe-based redox switch for tuning the acidity of a ZSM-5-based catalyst in the methanol-to-aromatics reaction. In this reaction, the yield of the target product, para-xylene (PX), is low because various types of acids on the catalyst activate side reactions. Fe oxides and zeolite generate medium-strength Lewis acids, which activate the aromatization of methanol but suppress the dealkylation of xylene. Gradual reduction of Fe oxides during the reaction simultaneously decreases the conversion of methanol, the yield of aromatics, and the yield of PX. The oxidation state of the Fe species and the associated catalytic performance can be regenerated in the air at 550 °C. The redox switches caused regular fluctuation in the catalytic performance and remained stable throughout 16 regeneration cycles (up to 80 h). The employed strategy enabled a PX yield of up to 60% (carbon base) using a SiO_2-coated Zn/P/Fe/ZSM-5 catalyst, which is 3–6 times higher than previously reported values. The result showed a new mode of acidity modulation of the catalyst.

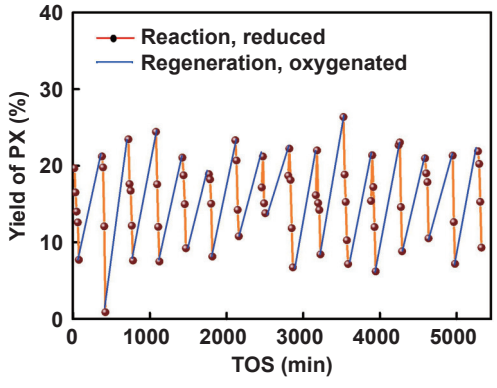

KEYWORDS: molecular switches, Fe, ZSM-5, methanol, para-xylene

1 Introduction

Molecular switches are molecules in which bonds, electronic state, or structure change in response to environmental stimuli such as light, heat, electrical field, pH, atmosphere, or pressure; they are widely used in photonics, bioscience, chiral synthesis, and computer science for logical calculations[1–8]. Although molecular switches have been widely employed in solutions and polymer systems, their use in heterogeneous catalysis to modulate the properties and performance of the catalyst has been rarely reported. For instance, para-xylene (PX), an important raw material for the production of synthetic fibers, is mainly produced via catalytic reforming of naphtha[9–11] and the methanol-to-aromatics (MTA) process catalyzed by M/ZSM-5 (M = Zn, Ga, Cu, Mo, Ni, etc)[11–22]. In general, strong acids on the catalyst result in side reactions, including dealkylation and isomerization of xylene (X), whereas weak acids lead to the alkylation of X to tri-methylbenzene (TriMB) or the poor performance of aromatization[9–33]. Owing to the very low yield of PX, < 10% (carbon base) in MTA and 3%–7% in catalytic reforming of naphtha, obtaining pure PX requires a complex transformation and separation network, which has one of the highest energy consumptions among all sections in any petrochemical process. Currently, isomerization of X can be effectively inhibited by minimizing the amount of external acids on the catalyst using coke or by coating the catalyst with a SiO_2 shell, which however sacrifices its aromatization ability[24–33]. Unfortunately, a strategy to simultaneously suppress the dealkylation of X to benzene (B) and toluene (T) on strong acids and the alkylation of X to TriMB on weak acids has not yet been reported owing to the acid-dependent aromatization ability of the catalys[15, 16, 21, 22].

In this work, we propose Fe-based redox switches to modulate the acidity of a ZSM-5-based catalyst. Similar to the use of H_2 to tune PdH_x states or the use of NO_x for turning Fe(II) or Fe(III) into complex molecules to improve the on–off sensitivity[1, 2], in the

Received: October 11, 2022; **Revised:** January 3, 2023
Accepted: January 19, 2023

✉Address correspondence to Chaojie Cui, cuicj06@tsinghua.edu.cn; Weizhong Qian, qianwz@tsinghua.edu.cn
#Qiongfang Hu and Hongmei Wang contributed equally to this work

https://doi.org/10.26599/CF.2023.9200001

present study, the redox state of the Fe species is controlled by the reaction atmosphere (hydrocarbons/H_2 reducing atmosphere) and catalyst regeneration (using air, oxidation). The modulation of acidity and acidic type through the redox state of Fe allows the suppression of not only the dealkylation of X (to T and B) on strong acids, but also the alkylation of X (to TriMB and other heavy components) on weak acids. We conducted 16 reaction–catalyst regeneration cycles (longer than 80 h in total) and recorded the trends in catalytic performance (including the conversion of methanol, the yield of aromatics, the yield of PX, and the selectivity of PX in X) determined directly by the redox switches. The results confirm the stability of Fe-based redox switches on the catalyst, providing new insights into the modulation of acidity and performance of the catalyst and providing new opportunities for designing a high-performance catalyst to directly produce PX from methanol. The increased yield of PX in the single pass conversion is expected to significantly decrease the energy consumption of downstream separation, considerably decreasing the carbon footprint of the process.

2 Experimental

First, the ZSM-5 catalyst was sequentially doped with Zn and P species to obtain Zn/P/ZSM-5. For Zn-doping, ZSM-5 powder was impregnated with $Zn(NO_3)_2$ solution, followed by drying at 110 °C for 24 h and calcination at 550 °C for 5 h (Supplementary SI-1). P-doping was performed following the same procedure, but using $(NH_4)_2HPO_4$ impregnation solution. Then, the obtained Zn/P/ZSM-5 catalyst was doped with Fe following the same procedure (but with $Fe(NO_3)_3$ impregnation solution) to prepare a Zn/P/Fe/ZSM-5 catalyst. External acids on the Zn/P/Fe/ZSM-5 catalyst were eliminated by coating the catalyst with a SiO_2 shell through the hydrolysis of TEOS, as previously described (Supplementary SI-1, Fig. S1)[24]. To test the performance of different catalysts in converting methanol into PX, the catalyst (around 1 g) was put into the vertically packed bed reactor. Methanol was fed into the reactor and catalytically converted at 475 °C and normal pressure for 2 h. The product of the reaction was analyzed using online gas chromatography at different reaction times. The deactivated catalyst was regenerated by feeding air to burn the coke at 550 °C for 3 h. A total of 16 reaction–catalyst regeneration cycles were run to test the stability of redox switches and record time-dependent catalytic performances.

3 Results and discussion

Considering that the effects of P-doping and SiO_2 layer have been well addressed previously[24,43], the present work mainly focuses on the effect of the addition of Fe species to the catalyst. Without doping with Fe species, only the lattice of ZSM-5 on the Zn/ZSM-5 catalyst is detected using transmission electron microscopy (TEM; Supplementary SI-1, Fig. S2), indicating that ZnO species are monodispersed on the ZSM-5 matrix. There is also a clear amorphous layer with a thickness of 6–8 nm, corresponding to the SiO_2 shell of the Zn/P/Fe/Si catalyst (Fig. 1a). However, this layer did not affect the detection of Fe-species nanoparticles. The doping of Zn/P/ZSM-5 with Fe species resulted in the formation of particles with the size of 2–5 nm on the catalyst. The typical lattice spacing of the crystal is 0.229 nm, as shown by high-resolution TEM (Fig. 1b), which was assigned to Fe_2O_3. Different lattice spacings (0.23 nm, 0.15 nm, etc.) associated with other Fe oxide phases are also observed in other regions of the catalysts sampled at 15 and 30 min after the start of the reaction (Figs. 1c and 1d). The elemental distribution in the catalyst, obtained by energy-dispersive X-ray spectroscopy (EDS), shows that the Fe species did not interact with the SiO_2 shell but interacted with the ZSM-5 (Supplementary SI-2, Fig. S3).

X-ray photoelectron spectroscopy (XPS) was used to determine the valence of Fe on different catalysts (Fig. 2a). In Fe/ZSM-5, not doped with Zn species, the peaks of Fe oxides at 710.2, 711.8, 714, and 719 eV were assigned to Fe^{2+} oct, Fe^{3+} oct, Fe^{3+} tet, and Fe^{3+} sat, respectively. These values correspond well to the previously reported data[34–44]. At the same time, in the Fe-doped Zn/P/ZSM-5, the peak of the Fe^{3+} tet species is relatively weak and blue-shifted

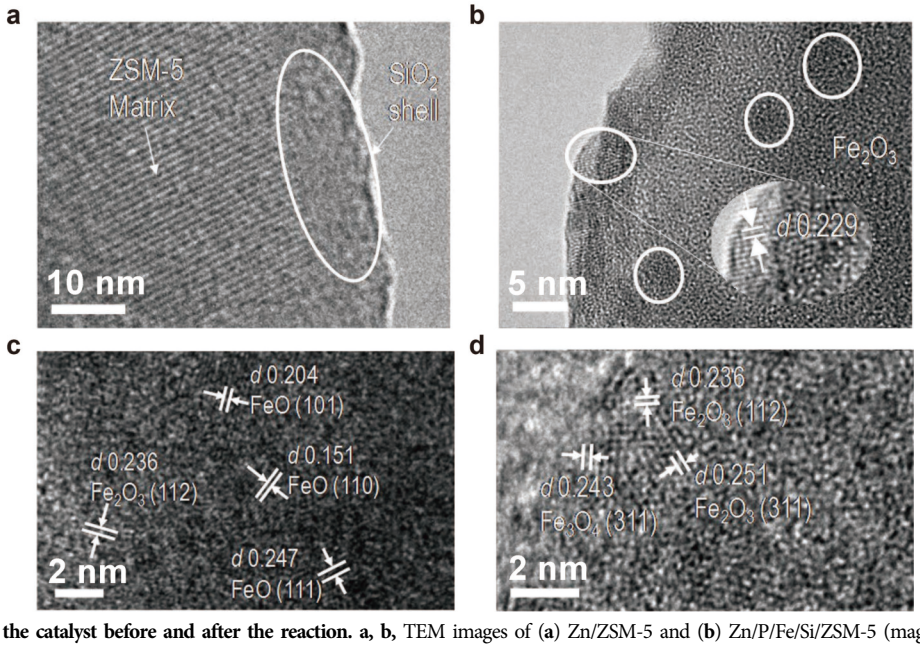

Fig. 1. TEM patterns of the catalyst before and after the reaction. a, b, TEM images of (**a**) Zn/ZSM-5 and (**b**) Zn/P/Fe/Si/ZSM-5 (magnified region showing Fe species). **c, d,** Lattice of Fe species on the catalyst after (**c**) 15 min of reaction and (**d**) 30 min of reaction.

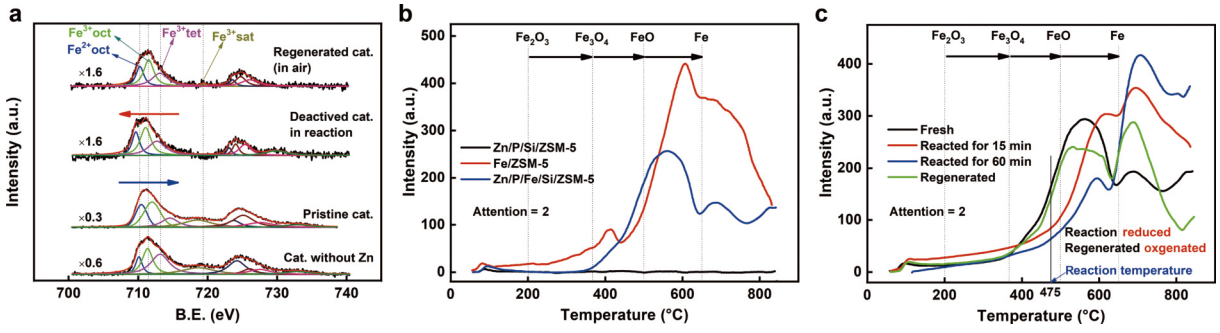

Fig. 2. XPS and TPR of Fe species on the catalyst. a, XPS of Fe species on the catalyst. **b**, TPR of different catalysts, where Fe/ZSM-5 has Fe loading of 6% and Zn/P/Fe/Si/ZSM-5 has Fe loading of nearly 4%. **c**, TPR of Zn/P/Fe/Si/ZSM-5 catalyst at different time points in reaction.

compared to those in samples without Zn. In contrast, in the patterns of catalysts sampled during the reaction, in the hydrocarbons/H_2 atmosphere, the peaks are redshifted. The reduction of Fe_2O_3 to Fe_3O_4 starts at 200 °C, the transformation of Fe_3O_4 into FeO occurs at 400 °C, and the reduction of FeO to metallic Fe occurs at 550 °C[34–36, 40–42]. Thus, Fe oxides on the catalyst are reduced in the MTA reaction at 475 °C. Notably, the catalysts containing Fe oxides, including Zn/P/Fe/Si/ZSM-5 and Fe/ZSM-5, show a sharp peak representing the consumption of H_2 in the temperature-programmed reduction (TPR) pattern (Fig. 2b), whereas Zn/P/Si/ZSM-5 does not. After the complete reduction of the catalysts containing Fe species, the peak area of H_2 consumption for Fe/ZSM-5 with Fe loading of 6% is around 1.5 times that for the Zn/P/Fe/Si/ZSM-5 catalyst with Fe loading of nearly 4%. This verifies that the state of Fe species on the catalyst is not significantly affected by the presence of Zn and P species. This conclusion is also confirmed by the XRD results (Supplementary SI-3, Fig. S4). Fe species are mainly comprised of hematite Fe_2O_3 (Supplementary SI-3, Fig. S4), which is in agreement with the XPS and TEM results and with most similar previous reports[34–44].

It should be noted that the P-doping of the catalyst performed after Zn-doping but before Fe-doping is effective for inhibiting the strong interaction between Fe and Zn species. In the absence of P-doping, strong interaction between Zn and Fe species results in a significant weakening of Fe peaks in the XRD pattern (Supplementary SI-3, Fig. S4). Furthermore, the above doping sequence did not allow the formation of large amounts of $ZnFe_2O_4$ species on the catalyst, whose signal overlaps with that of ZnO species in the XPS pattern (Supplementary SI-4, Fig. S5). In addition, catalysts that reacted for 15 and 60 min at 475 °C in MTA (Fig. 2c) both show a peak response (consumption of H_2) in the TPR pattern. However, the peak area after 60 min of reaction is smaller than that after 15 min of reaction, validating the gradual reduction of Fe oxides during MTA and the presence of Fe oxides on the catalyst even after reacting for 60 min. After 105 min of MTA, the deactivated catalyst was regenerated by burning coke in the air at 550 °C. During regeneration, Fe, and FeO species were converted to Fe_2O_3 and Fe_3O_4 again, resulting in the appearance of an intensive peak of H_2 consumption in the TPR pattern (Fig. 2c). The position of this peak in the regenerated catalyst closely coincides with that in the pristine catalyst.

Effects of the transition of Fe(III) oxides to Fe(II) oxides or even metallic Fe at 475 °C on the performance of the catalyst in MTA (Figs. 2b and 2c) were examined. The Zn/P/Fe/ZSM-5 catalyst containing Fe oxides exhibits high conversion of methanol (close to 100%), high yield of aromatics (60%–65%, carbon base), high yield of PX (20%, carbon base), and low selectivity of PX in X (50%) in the initial stage of the reaction (Fig. 3). As the reaction proceeds, Fe oxides are gradually reduced, resulting in the decrease in catalytic performance. Quantitatively, the yield of PX decreases from 20%–25% at 15 min to approximately 8% at 60 min. At the same time, the conversion of methanol drops from 100% to 70%, and the yield of aromatics decreases from 65% to 20%. Only the selectivity of PX in X increases from 50% to 75%, because the isomerization of X was suppressed by the weakening of the external acids by coke[24]. However, all these decreases are recovered after the regeneration of the catalyst by burning coke in the air at 550 °C. Sixteen

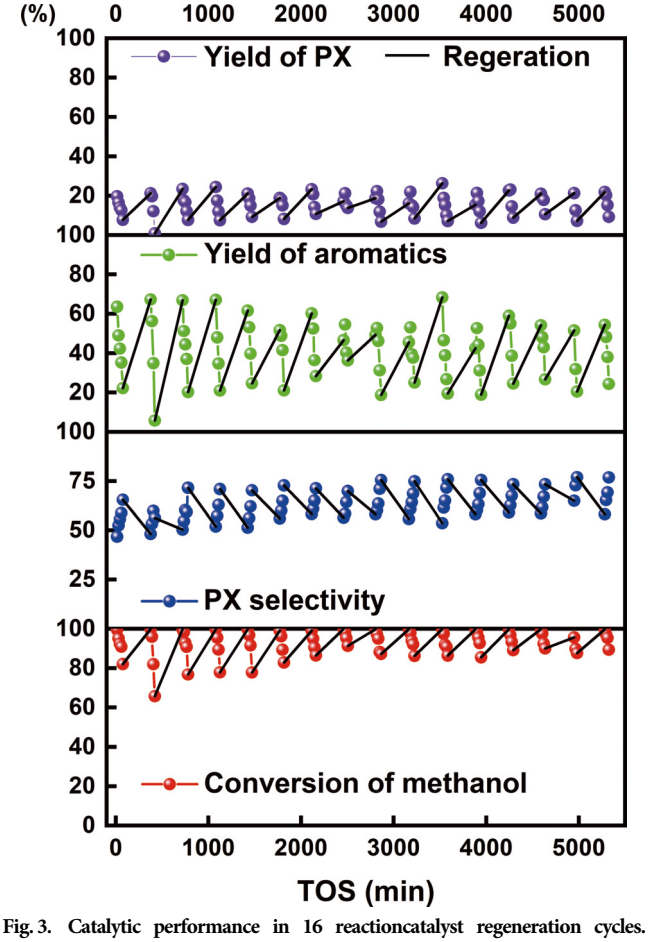

Fig. 3. Catalytic performance in 16 reactioncatalyst regeneration cycles. Redox state of Fe species governing the regular fluctuation in catalytic performance in 16 reaction–catalyst regeneration cycles, using Zn/P/Fe/ZSM-5 catalyst (Si/Al ratio in ZSM-5 is 19). Black lines indicate the regeneration of the catalyst in the air at 550 °C. Colored points represent the experimental data in the MTA reaction in a hydrocarbons/H_2 atmosphere.

reaction–catalyst regeneration cycles show regular decreasing and increasing trends in methanol conversion, aromatic yield, PX selectivity (in an opposite direction), and PX yield modulated by the redox molecular switches of Fe species on the catalyst. Notably, the peak Fe species levels of the regenerated catalyst show a close correlation with those of the fresh catalyst over the 16 reaction cycles, but the peak levels of the two are not equal, indicating that Fe species on the catalyst reached the equilibrium rather than the initial state in the successive regenerations (Supplementary SI-5, Fig. S6). Consistent recovery of catalytic performance throughout 16 cycles confirms the high stability of the proposed redox switches.

Infrared spectroscopy of pyridine adsorption (Py-IR; Supplementary SI-6, Fig. S7) was used to characterize the acidic types of the catalysts containing Fe-based redox switches. The peak at 1540 cm^{-1} in the Py-IR pattern of Zn/P/Si/ZSM-5 (Supplementary SI-6, Fig. S7), assigned to a large amount of Bronsted acids, nearly disappears after Fe-doping. At the same time, the peak at 1450 cm^{-1}, assigned to Lewis acids, becomes very intense. In addition, calcination in air at a higher temperature (550–750 °C) during Fe-doping increases the intensity of the peak of Lewis acids (Supplementary SI-6, Fig. S8). These results confirm that Lewis acids were generated through the interaction of Fe oxides with ZSM-5. Moreover, coating the catalyst with a SiO_2 shell did not change the position of Lewis acids and pore structure (Supplementary SI-7, Fig. S9). This suggests that the Fe species mainly interacted with the zeolite, not the SiO_2 shell, which is in agreement with the EDS results. The results of temperature-programmed desorption of ammonia (NH_3-TPD) suggest that the addition of Fe oxides to Zn/P/Si/ZSM-5 increased the strength of all types of acids (Supplementary SI-8, Table S1). This is reasonable considering that Fe oxides mostly interacted with zeolite, not ZnO (Supplementary SI-8, Fig. S10), to create new sites of Bronsted acids and Lewis acids. At the same time, the acidic density of the catalyst drastically decreases in the first 15 min of the MTA reaction, as shown by NH_3-TPD (Fig. 4a). Afterwards (from 30 to 60 min), it decreases nearly linearly with a relatively low slope. The same trend is observed for strong, medium-strong, and weak acids, owing to the gradual reduction of Fe species and gradual deposition of coke. As expected, the decrease in acid density directly affected the aromatic distribution (Fig. 4b). In the initial 15 min of reaction, the yields of T and B are 36.1% and 7.55%, respectively, while the yield of PX is only 26.6%. Apparently, high acid strength and density in the catalyst resulted in the dealkylation of X to T and B. However, the amount of strong acids drops much faster than those of other acids, resulting in a decrease in the yield of T to 4.98% at 30 min and an increase in the yield of PX to 59.9% (carbon base). The selectivity of PX among all aromatics at 30 min is up to 85%. The progressing reduction of Fe oxides further decreases the acidity at 45 min, when the dealkylation of X nearly stops; however, significant alkylation of X to TriMB is observed. Similarly, the decrease in acidic density with the reaction time is observed for Zn/P/Si/ZSM-5 without Fe species, on which the dealkylation of X to T and B also readily occurs in the initial 15 min. However, a further decrease in acidic strength at 45–75 min results in a significant loss of the aromatization activity of the catalyst, although the selectivity of PX in X remains high (Fig. 4c). These results clearly show that the yield of PX is directly determined by the redox switches of Fe species with a tunable amount, type, and strength of acids. Similar to the regular decrease and increase in the catalytic performance during cycling in Fig. 3, the acidic density of the catalyst considerably decreases in the first reaction cycle but is recovered to a certain degree after the regeneration of the catalyst (Supplementary SI-8, Fig. S11). However, the acid strength in the second reaction cycle decreases faster than the associated catalytic performance, which needs further investigation. It should be noted that only the coating of the catalyst with a SiO_2 shell suppressed the isomerization of X on the external surface, which made the effect of Fe-based redox switches significant. When using the Zn/P/Fe/catalyst without the SiO_2 shell, the selectivity of PX in X is only 40%–60% (Fig. 3); however, the effect of redox switches is observed even in this case. To the best of our knowledge, this is the first report of the yield of PX approaching 60% in a single pass, which is 3–6 times higher than the previously reported yields for MTA and 5–10 times higher than those for catalytic reforming of naphtha[9–33]. Thus, a high yield of PX may be attained by shortening the reaction time in the reaction–catalyst regeneration cycles using the redox switches mechanism.

4 Conclusions

We report a multicomponent catalyst, Zn/P/Fe/ZSM-5@SiO_2, for the one-step conversion of methanol to PX. The presence of Fe-based redox switches on the zeolite-based catalyst was confirmed by XPS, TPR, Py-IR, and catalytic performance in MTA. The reported catalytic effect is stable, as shown in 16 repeated reaction–catalyst regeneration cycles up to 80 h. The present results provide new insights into the use of redox switches in heterogeneous catalysis and into the design and control of the catalysts with moderate acidic properties for obtaining the desired activity, product selectivity, and yield simultaneously.

Acknowledgements

This work is finically supported by the National Natural Science Foundation of China (22278236) and the National Key Research and Development Program of China (2020YFB0606401).

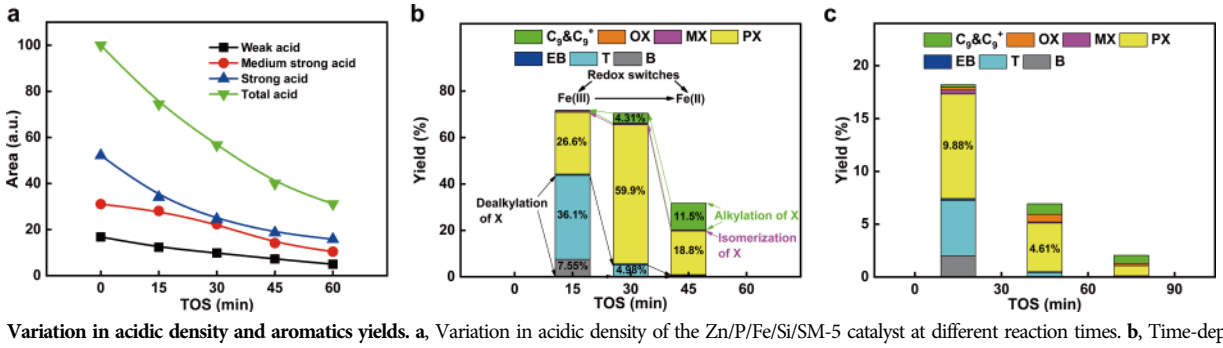

Fig. 4. Variation in acidic density and aromatics yields. a, Variation in acidic density of the Zn/P/Fe/Si/SM-5 catalyst at different reaction times. **b**, Time-dependent yield of different aromatics with the Zn/P/Fe/Si/ZSM-5 catalyst. **c**, Time-dependent yield of different aromatics with the Zn/P/Si/ZSM-5 catalyst without Fe.

Author contributions

Q.F.H. and H.M.W. contributed equally to this work. W.Z.Q. initiated and led the whole project. W.Z.Q. and C.J.C. supervised and coordinated the project. Q.F.H. prepared all catalysts and carriedout catalytic tests and some characterization measurements. H.M.W. performed XPS, TPR and BET measurements and analyzed the results. Q.F.H. and H.M.W. wrote the first draft. All authors discussed the results and improved the manuscript.

Competing interests

The authors declare no competing financial interests.

Additional information

Supplementary information The online version contains supplementary material available at https://doi.org/10.26599/CF.2023.9200001.

References

[1] Wang, S. H.; Han, M. Y.; Huang, D. J. Nitric oxide switches on the photoluminescence of molecularly engineered quantum dots. *J. Am. Chem. Soc.* **2009**, *131*, 11692–11694.

[2] Dasari, R.; Zamborini, F. P. Hydrogen switches and sensors fabricated by combining electropolymerization and Pd electrodeposition at microgap electrodes. *J. Am. Chem. Soc.* **2008**, *130*, 16138–16139.

[3] Fioravanti, G.; Haraszkiewicz, N.; Kay, E. R.; Mendoza, S. M.; Bruno, C.; Marcaccio, M.; Wiering, P. G.; Paolucci, F.; Rudolf, P.; Brouwer, A. M. et al. Three state redox-active molecular shuttle that switches in solution and on a surface. *J. Am. Chem. Soc.* **2008**, *130*, 2593–2601.

[4] Wang, Y.; Tan, X.; Zhang, Y. M.; Zhu, S. Y.; Zhang, I.; Yu, B. H.; Wang, K.; Yang, B.; Li, M. J.; Zou, B. et al. Dynamic behavior of molecular switches in crystal under pressure and its reflection on tactile sensing. *J. Am. Chem. Soc.* **2015**, *137*, 931–939.

[5] Belhboub, A.; Boucher, F.; Jacquemin, D. Grafting spiropyran molecular switches on TiO_2: A first-principles study. *J. Phys. Chem. C* **2016**, *120*, 18281–18288.

[6] Niroui, F.; Wang, A. I.; Sletten, E. M.; Song, Y.; Kong, J.; Yablonovitch, E.; Swager, T. M.; Lang, J. H.; Bulovic, V. Tunneling nanoelectromechanical switches based on compressible molecular thin films. *ACS Nano* **2015**, *9*, 7886–7894.

[7] Simpson, G. J.; Hogan, S. W. L.; Caffio, M.; Adams, C. J.; Früchtl, H.; van Mourik, T.; Schaub, R. New class of metal bound molecular switches involving H-tautomerism. *Nano Lett.* **2014**, *14*, 634–639.

[8] Ohtake, T.; Tanaka, H.; Matsumoto, T.; Kimura, M.; Ohta, A. Redox-driven molecular switches consisting of bis(benzodithiolyl)bithienyl scaffold and mesogenic moieties: Synthesis and complexes with liquid crystalline polymer. *J. Org. Chem.* **2014**, *79*, 6590–6602.

[9] Ali, S. A.; Siddiqui, M. A.; Ali, M. A. Parametric study of catalytic reforming process. *React. Kinet. Catal. Lett.* **2005**, *87*, 199–206.

[10] Coppens, M. O.; Froment, G. F. Fractal aspects in the catalytic reforming of naphtha. *Chem. Eng. Sci.* **1996**, *51*, 2283–2292.

[11] Sotelo-Boyas, R.; Froment, G. F. Fundamental kinetic modeling of catalytic reforming. *Ind. Eng. Chem. Res.* **2009**, *48*, 1107–1119.

[12] Adebajo, M. O.; Long, M. A. The contribution of the methanol-to-aromatics reaction to benzene methylation over ZSM-5 catalysts. *Catal. Commun.* **2003**, *4*, 71–76.

[13] Zaidi, H. A.; Pant, K. K. Catalytic conversion of methanol to gasoline range hydrocarbons. *Catal. Today* **2004**, *96*, 155–160.

[14] Lalik, E.; Liu, X. S.; Klinowski, J. Role of gallium in the catalytic activity of zeolite [Si, Ga]-Zsm-5 for methanol conversion. *J. Phys. Chem.* **1992**, *96*, 805–809.

[15] Wang, T.; Tang, X. P.; Huang, X. F.; Qian, W. Z.; Cui, Y.; Hui, X. Y.; Yang, W.; Wei, F. Conversion of methanol to aromatics in fluidized bed reactor. *Catal. Today* **2014**, *233*, 8–13.

[16] Zhang, J. G.; Qian, W. Z.; Tang, X. P.; Shen, K.; Wang, T.; Huang, X. F.; Wei, F. Influence of catalyst acidity on dealkylation, isomerization and alkylation in MTA process. *Acta Phys. Chim. Sin.* **2013**, *29*, 1281–1288.

[17] Wang, N.; Qian, W. Z.; Wei, F. Fabrication and catalytic properties of three-dimensional ordered zeolite arrays with interconnected micro-meso-macroporous structure. *J. Mater. Chem. A* **2016**, *4*, 10834–10841.

[18] Zhou, J.; Teng, J. W.; Ren, L. P.; Wang, Y. D.; Liu, Z. C.; Liu, W.; Yang, W. M.; Xie, Z. K. Full-crystalline hierarchical monolithic ZSM-5 zeolites as superiorly active and long-lived practical catalysts in methanol-to-hydrocarbons reaction. *J. Catal.* **2016**, *340*, 166–176.

[19] Ilias, S.; Bhan, A. Mechanism of the catalytic conversion of methanol to hydrocarbons. *ACS Catal.* **2013**, *3*, 18–31.

[20] Olsbye, U.; Svelle, S.; Bjorgen, M.; Beato, P.; Janssens, T. V. W.; Joensen, F.; Bordiga, S.; Lillerud, K. P. Conversion of methanol to hydrocarbons: How zeolite cavity and pore size controls product selectivity. *Angew. Chem., Int. Ed.* **2012**, *51*, 5810–5831.

[21] Shen, K.; Qian, W.; Wang, N.; Su, C.; Wei, F. Fabrication of *c*-axis oriented ZSM-5 hollow fibers based on an *in situ* solid-solid transformation mechanism. *J. Am. Chem. Soc.* **2013**, *135*, 15322–15325.

[22] Shen, K.; Qian, W. Z.; Wang, N.; Zhang, J. G.; Wei, F. Direct synthesis of *c*-axis oriented ZSM-5 nanoneedles from acid-treated kaolin clay. *J. Mater. Chem. A* **2013**, *1*, 3272–3275.

[23] Wang, N.; Qian, W. Z.; Shen, K.; Su, C.; Wei, F. Bayberry-like ZnO/MFI zeolite as high performance methanol-to-aromatics catalyst. *Chem. Commun. (Camb.)* **2016**, *52*, 2011–2014.

[24] Zhang, J. G.; Qian, W. Z.; Kong, C. Y.; Wei, F. Increasing para-xylene selectivity in making aromatics from methanol with a surface-modified Zn/P/ZSM-5 catalyst. *ACS Catal.* **2015**, *5*, 2982–2988.

[25] Ahn, J. H.; Kolvenbach, R.; Al-Khattaf, S. S.; Jentys, A.; Lercher, J. A. Enhancing shape selectivity without loss of activity-novel mesostructured ZSM5 catalysts for methylation of toluene to p-xylene. *Chem. Commun. (Camb.)* **2013**, *49*, 10584–10586.

[26] Young, L. B.; Butter, S. A.; Kaeding, W. W. Shape selective reactions with zeolite catalysts: III. Selectivity in xylene isomerization, toluene-methanol alkylation, and toluene disproportionation over ZSM-5 zeolite catalysts. *J. Catal.* **1982**, *76*, 418–432.

[27] Mirth, G.; Cejka, J.; Lercher, J. A. Transport and isomerization of xylenes over HZSM-5 zeolites. *J. Catal.* **1993**, *139*, 24–33.

[28] Kaeding, W. W.; Chu, C.; Young, L. B.; Weinstein, B.; Butter, S. A. Selective alkylation of toluene with methanol to produce para-xylene. *J. Catal.* **1981**, *67*, 159–174.

[29] Kim, J. H.; Namba, S.; Yashima, T. Para-selectivity of zeolites with MFI structure: Difference between disproportionation and alkylation. *Appl. Catal. A Gen.* **1992**, *83*, 51–58.

[30] Ivanova, I. I.; Corma, A. Surface species formed and their reactivity during the alkylation of toluene by methanol and dimethyl ether on zeolites as determined by *in situ* ^{13}C MAS NMR. *J. Phys. Chem. B* **1997**, *101*, 547–551.

[31] Zheng, S.; Heydenrych, H. R.; Röger, H. P.; Jentys, A.; Lercher, J. A. On the enhanced selectivity of HZSM-5 modified by chemical liquid

deposition. *Top. Catal.* **2003**, *22*, 101–106.

[32] Wang, I.; Ay, C. L.; Lee, B. J.; Chen, M. H. Para-selectivity of dialkylbenzenes over modified HZSM-5 by vapour phase deposition of silica. *Appl. Catal.* **1989**, *54*, 257–266.

[33] Miyake, K.; Hirota, Y.; Ono, K.; Uchida, Y.; Tanaka, S.; Nishiyama, N. Direct and selective conversion of methanol to para-xylene over Zn ion doped ZSM-5/silicalite-1 core–shell zeolite catalyst. *J. Catal.* **2016**, *342*, 63–66.

[34] Lubango, L. M.; Scurrell, M. S. Light alkanes aromatization to BTX over Zn-ZSM-5 catalysts: Enhancements in BTX selectivity by means of a second transition metal ion. *Appl. Catal. A Gen.* **2002**, *235*, 265–272.

[35] Perez-Ramírez, J.; Kumar, M. S.; Brückner, A. Reduction of N_2O with CO over FeMFI zeolites: Influence of the preparation method on the iron species and catalytic behavior. *J. Catal.* **2004**, *223*, 13–27.

[36] Ma, A. Z.; Grünert, W. Selective catalytic reduction of NO by ammonia over Fe-ZSM-5 catalysts. *Chem. Commun.* **1999**, *1*, 71–72.

[37] Tan, P. L. Active phase, catalytic activity, and induction period of Fe/zeolite material in nonoxidative aromatization of methane. *J. Catal.* **2016**, *338*, 21–29.

[38] Weckhuysen, B. M.; Wang, D. J.; Rosynek, M. P.; Lunsford, J. H. Conversion of methane to benzene over transition metal ion ZSM-5 zeolites: II. Catalyst characterization by X-ray photoelectron spectroscopy. *J. Catal.* **1998**, *175*, 347–351.

[39] Shwan, S.; Nedyalkova, R.; Jansson, J.; Korsgren, J.; Olsson, L.; Skoglundh, M. Hydrothermal stability of Fe-BEA as an NH_3-SCR catalyst. *Ind. Eng. Chem. Res.* **2012**, *51*, 12762–12772.

[40] Jozwiak, W. K.; Kaczmarek, E.; Maniecki, T. P.; Ignaczak, W.; Maniukiewicz, W. Reduction behavior of iron oxides in hydrogen and carbon monoxide atmospheres. *Appl. Catal. A Gen.* **2007**, *326*, 17–27.

[41] Kang, S. H.; Bae, J. W.; Sai Prasad, P. S.; Jun, K. W. Fischer–Tropsch synthesis using zeolite-supported iron catalysts for the production of light hydrocarbons. *Catal. Lett.* **2008**, *125*, 264–270.

[42] Jin, Y. M.; Datye, A. K. Phase transformations in iron Fischer–Tropsch catalysts during temperature-programmed reduction. *J. Catal.* **2000**, *196*, 8–17.

[43] Wang, N.; Li, J.; Sun, W. J.; Hou, Y. L.; Zhang, L.; Hu, X. M.; Yang, Y. F.; Chen, X.; Chen, C. M.; Chen, B. H. et al. Rational design of zinc/zeolite catalyst: Selective formation of p-xylene from methanol to aromatics reaction. *Angew. Chem., Int. Ed.* **2022**, *61*, e202114786.

[44] Torres Galvis, H. M.; Bitter, J. H.; Davidian, T.; Ruitenbeek, M.; Dugulan, A. I.; de Jong, K. P. Iron particle size effects for direct production of lower olefins from synthesis gas. *J. Am. Chem. Soc.* **2012**, *134*, 16207–16215.